RAPID COMMUNICATIONS IN MASS SPECTROMETRY
Rapid Commun. Mass Spectrom. 2005; **19**: 2528–2538
Published online in Wiley InterScience (www.interscience.wiley.com). DOI: 10.1002/rcm.2087

RCM

Examining the collision-induced decomposition spectra of ammoniated triglycerides as a function of fatty acid chain length and degree of unsaturation. I. The OXO/YOY series

Xingwen Li and Jason J. Evans*
Chemistry Department, University of Massachusetts Boston, Boston, MA 02125, USA

Received 2 June 2005; Revised 11 July 2005; Accepted 11 July 2005

A series of positionally pure triglycerides (TAGs) of the form OXO and YOY, where O is the oleate moiety and X and Y are large arrays of different fatty acid moieties, was synthesized and analyzed by reversed-phase high-performance liquid chromatography/tandem mass spectrometry. The intensities of the collision-induced decomposition (CID) products of ammoniated TAGs (ammonium ion adducts) were examined as a function of chain length, degree of unsaturation, double-bond position, and *cis*/*trans* configuration of X and Y. The major CID products, the diglyceride fragment ions and the MH^+ ion, were plotted as functions of chain length for the saturated and mono-unsaturated series of X and Y. Different trends for each of these series were observed. Trends in the abundances of these fragment ions were also characterized as a function of degree of unsaturation in the TAGs. In general, the fractional abundances of the MH^+ ions vary linearly with degree of unsaturation. However, the presence of double bonds positioned close to the carbonyl carbon of the fatty acid chain promotes the formation of the diglyceride fragment ion corresponding to loss of that fatty acid. Mechanisms of the formation and decomposition of ammoniated TAGs are proposed that fit the trends observed in the data. Extensions of this work are described, and a vision of a derived library of CID spectra is discussed as a platform for comprehensive analysis of complex TAG mixtures. Copyright © 2005 John Wiley & Sons, Ltd.

Absorption[1–5] and metabolism[6–13] of dietary triglycerides (TAGs) depend on stereochemical configuration. As a result, the positional arrangement of the fatty acid moieties in TAGs has an impact on an array of lipotoxic diseases,[14–21] such as heart disease, obesity, and diabetes. Development of efficient methods for the positional analysis of TAGs is needed to facilitate research in these areas, as well as in the area of basic nutrition. In addition, there is a growing interest in designing lipids to increase functionality, while maintaining lower levels of saturated and *trans*-fatty acid content in food products. The processes used in lipid design often require rearrangement of the fatty acid moieties along the glycerol backbone. Positional analysis will be needed to confirm the compositions of these designer lipid products.

Recently, methods based on reversed-phase high-performance liquid chromatography coupled with atmospheric pressure chemical ionization mass spectrometry (RP-HPLC/APCI-MS),[22–29] and on RP-HPLC coupled with electrospray ionization tandem mass spectrometry (HPLC/ESI-MS/MS),[30–33] have been developed for positional analysis of TAGs. These methods are less laborious than traditional methods[34–46] that require fractionation of TAGs, fraction collection, enzymatic digestion of each fraction, and the separation and detection of the diglycerides (DAGs) and free fatty acid hydrolysis products in each of the digested fractions. RP-HPLC provides superb fractionation of complex TAG mixtures, and on-line mass spectrometric analysis yields information about fatty acid composition and position. The *m*/*z* ratios of the DAG fragment ions provide fatty acid composition data, and relative abundances of the DAG fragment ions provide positional data. It has been well established with both the ESI-MS/MS and the APCI-MS methods that loss of the fatty acid in the center position is unfavorable.[25,47,48] Thus, the positional assignment has generally been based on the DAG fragment ion of lowest abundance.

However, positional analysis is more complex when samples contain mixtures of positional isomers. Positional isomers co-elute in traditional RP-HPLC, and an average collision-induced decomposition (CID) spectrum across the chromatographic peak corresponding to a given system of positional isomers is a composite spectrum based on the relative abundances of the positional isomers in the sample. It is possible to retrieve the relative abundance data from this composite CID spectrum.

**Correspondence to*: J. J. Evans, Chemistry Department, University of Massachusetts Boston, 100 Morrissey Boulevard, Boston, MA 02188, USA.
E-mail: Jason.evans@umb.edu
Contract/grant sponsor: The American Chemical Society Petroleum Research Fund.

Using RP-HPLC/ESI-MS/MS on the ammonium ion adducts of a limited number of positional isomer systems (SOS/SSO, OSO/OOS, and POS/PSO/SPO, where O, S, and P are the oleate, stearate, and palmitate fatty acid moieties), we have shown that standard calibration plots can be produced that enable the determination of fractional compositions of binary mixtures of position isomers;[31] Fauconnot has reported similar work with several TAG systems of various degrees of unsaturation.[29] These works have established a linear relationship between the relative abundances of the DAG fragment ions and the relative proportions of regioisomers within a positional isomer system. For comprehensive analysis of complex mixtures using this approach, the fragmentation patterns of all pertinent TAG standards in a complex mixture must be known or at least predictable. To this end, we aim to synthesize several series of positionally pure TAGs that will enable the development of a model for predicting fragmentation patterns and eventually lead to the development of a derived library of CID spectra for TAGs that will be useful for the comprehensive analysis of complex TAG mixtures. This paper reports on the initial phase of this project.

Two different TAG designations will be used throughout this paper. The first designation, which is reserved specifically for oleic acid, is the letter 'O'. All other fatty acids will be designated using the following format: $C_{m:n}$, where 'm' indicates the carbon number of the fatty acid chain length, and 'n' indicates the degree of unsaturation for the fatty acid. Information about double-bond position and *cis*/*trans* orientation will be given in parentheses after n. For example, the TAG that consists of two *cis*-9-hexadecenate constituents in the outer positions and an oleate constituent in the center position is designated as $C_{16:1(c\text{-}9)}OC_{16:1(c\text{-}9)}$. The middle designation indicates which fatty acid is in the center position. No distinction is made between the outer positions.

EXPERIMENTAL

Optima-grade methanol, 2-propanol, and chloroform were purchased from Fisher Scientific (Pittsburgh, PA, USA). Ammonium formate (99%) was purchased from Acros (Morris Plains, NJ, USA). Standard positional isomers of TAGs were purchased from Larodan (Malmo, Sweden), and were greater than 98% pure. These standard TAGs included $C_{18:0}OC_{18:0}$, $C_{18:0}C_{18:0}O$, $OC_{18:0}O$, $OOC_{18:0}$, $C_{16:0}OC_{16:0}$, $C_{16:0}C_{16:0}O$, $C_{24:0}OC_{24:0}$, $C_{12:0}OC_{12:0}$, $C_{8:0}OC_{8:0}$, $OC_{24:0}O$, $OC_{12:0}O$, $OC_{8:0}O$, $C_{18:0}OC_{16:0}$, and $C_{20:0}OC_{16:0}$. Various fatty acid chlorides and 1,3-DAGs were purchased from Nu-Chek Prep, Inc. (Elysian, MN, USA). The positional purities of the 1,3-DAGs were listed as greater than 99% pure. 4-Dimethylaminopyridine (DMAP, the base used in acylation reactions) and 2-oleoylglycerol were purchased from Sigma (St. Louis, MO, USA).

Synthesis

We have synthesized a series of positionally pure TAGs with the composition YXY. In this initial report we focus on two series, YOY and OXO, where O represents the oleate moiety $C_{18:1(c\text{-}9)}$, and X and Y represent a large series of different fatty acids that were chosen to investigate the effects of carbon chain length, degree of unsaturation, *cis*/*trans* configuration, and double-bond position on the relative abundances of the DAG fragment ions and the MH^+ ions.

TAGs of composition YXY were synthesized as follows. A 1,3-YY DAG (4 μmol) was added to a 3 mL vial wrapped in aluminum foil and dissolved in 1.0 mL of chloroform. Then, 1 mg of DMAP was added and the mixture was stirred using a small stirring bar. Then the X-fatty acid chloride (4 μmol) was slowly added dropwise with continuous stirring. The mixture was stirred for 30 min and then diluted (×100) with methanol saturated with ammonium formate; the reaction products were then analyzed by RP-HPLC/MS/MS or stored in the freezer for future analysis. The TAG product of the reaction was either OXO or YOY. Generally, we synthesized several TAGs (up to 15) in a single batch by either adding a mixture of fatty acid chlorides to 1,3-diolein or a mixture of 1,3-DAGs to the oleoyl ($C_{18:1(c\text{-}9)}$) fatty acid chloride. The molar ratio of DAG to fatty acid chloride was adjusted such that all of the reactants were potentially exhausted during the reaction. The TAGs chosen for a given synthesis were selected such that each could be analyzed efficiently in a single HPLC/MS/MS run. For instance, a batch of OXO TAGs was synthesized by slowly adding a mixture consisting of 11 fatty acid chlorides ranging from $C_{14:0}$ to $C_{24:0}$ (4 μmol each) to a 1.0 mL solution containing 44 μmol of 1,3-diolein and 1 mg of DMAP. The resulting mixture of 11 OXO-type TAGs was efficiently separated and analyzed by RP-HPLC/ESI-MS/MS.

Several YOX-type TAGs were synthesized from 2-oleoylglycerol, fatty acid chlorides, and DMAP. These YOX-type TAGs were used as standards to explore the possibility of using the trends observed in the OXO/YOY data for predicting the CID spectra of YOX-type TAGs. This synthesis was similar to that described above. Aliquots of 4 μmol each of 2-oleoylglycerol, the X fatty acid chloride, and the Y fatty acid chloride were used in the preparation of each of these YOX TAGs. For instance, the synthesis of $C_{18:2(cc\text{-}9,12)}OC_{18:0}$ was achieved by slowly adding a mixture consisting of 4 μmol of the $C_{18:2(cc\text{-}9,12)}$ fatty acid chloride and 4 μmol of the $C_{18:0}$ fatty acid chloride to a solution containing 4 μmol of 2-oleoylglycerol and 1 mg of DMAP. This reaction produced a mixture of $C_{18:2(cc\text{-}9,12)}OC_{18:0}$, $C_{18:0}OC_{18:0}$, and $C_{18:2(cc\text{-}9,12)}OC_{18:2(cc\text{-}9,12)}$. These TAGs were easily separated and analyzed upon analysis by RP-HPLC/ESI-MS/MS.

Standard solutions of each of the TAGs purchased from Larodan were prepared in 2-propanol at concentrations of 100 ± 2 μM. Diluted standards (10.00 μM) for each were prepared in methanol saturated with ammonium formate. The MS/MS spectra of the ammonium ion adducts of these diluted standards were used to assess the positional purity of the TAG products from the syntheses, as well as to assess the effectiveness of using the data produced from the OXO and YOY series of TAGs to predict fragmentation patterns of other TAG species. Each synthesis described above contained at least one TAG that matched one of these purchased standards. This served as an internal check for monitoring the purity of the synthesized positional isomers.

Mass spectrometer parameters

An LCQ Advantage ion trap mass spectrometer (Thermo-Electron, Sunnyvale, CA, USA) was used to detect and

RCM

characterize the TAGs. The connection from the HPLC column to the ESI source was made through a 1/16″ stainless steel zero-dead volume union and a 30 cm long, 50 μm i.d., 185 μm o.d. segment of fused-silica capillary. The end of the fused-silica capillary was fed into the ESI interface through a metal sheath. The tip of the capillary was carefully cut to provide a uniformly shaped tip, and was positioned so that it was at the edge of the metal sheath. The operating parameters of the ion trap mass spectrometer were as follows; capillary temperature 280°C, spray voltage 4.00 kV, and sheath gas 30 cm^3/min. CID of the TAG ammonium ion adducts was performed at a relative collision energy of 30 (unitless quantity). This value should be applicable to other LCQ systems, assuming that the instrumental calibration procedures described by the manufacturer are carefully followed. These experiments were not ultra-sensitive to the collision energy; the relative proportions among the DAG fragment ions and the MH^+ ion remain essentially constant at collision energies in the range of 25–35 (arbitrary units).

The instrument was primarily operated in the data-dependent MS/MS mode. In this mode the instrument alternates between collecting full-scan mass spectra and data-dependent CID spectra. The most intense ion in the full-scan mass spectrum is selected for isolation and CID in obtaining the subsequent data-dependent MS/MS scan. On a few occasions, two of the TAGs in one of our synthetic mixtures co-eluted. For these samples the analyses were repeated using a targeted MS/MS experiment. In this mode the instrument was programmed to perform CID on ions at a specific m/z ratio corresponding to the TAG component of lower intensity that was missed in the data-dependent analysis.

HPLC parameters

A low-flow Shimadzu (Kyoto, Japan) HPLC system, which included a SCL-10A vp controller, two LC-10AD vp pumps, a SIL-10AD vp auto injector, and a 10 cm, 1 mm i.d., 3 μm particle size, C_{18} BetaBasic reversed-phase column (ThermoElectron), was used to separate the TAGs. The HPLC system was operated at a flow rate of 30 μL/min. A gradient elution was utilized, consisting of mobile phase A (methanol/2-propanol, 80:20, v/v, saturated with ammonium formate) and B (2-propanol, saturated with ammonium formate). The binary gradient was as follows: 0 min/0% B, 4 min/10% B, 36 min/60% B, 38–40 min/85% B. Injection volume was 5 μL for all samples (approx. 50–200 pmol of TAG on-column).

Data analysis

The relative abundances of the DAG fragment ions and the MH^+ ions in the CID spectra of the ammoniated synthesized TAGs were entered into a spreadsheet for analysis. The relative abundances were converted into 'fractional intensities'. In this paper the term 'fractional intensity' of a given CID product refers to the relative abundance of the CID product divided by the sum of the relative abundances of the two DAG fragment ions and the MH^+ ion. For instance, if the relative abundances of YY^+, YX^+, and MH^+ in the CID spectrum of an YXY TAG are 0.20, 1.0, and 0.30, the calculated fractional intensities of these ions are 0.13, 0.67, and 0.20, respectively.

The term 'significantly' is also used throughout this manuscript. It implies that the statement has passed a t-test at the 95% confidence limit (CL). For instance, the phrase 'the fractional intensities of the OO^+ increased significantly as a function of chain length' means that the slope of the regression line for the plot of fractional intensity of OO^+ vs. chain length was greater than zero to the 95% CL.

Determination of positional purity

Calibration curves for the $C_{18:0}OC_{18:0}/C_{18:0}C_{18:0}O$, $OC_{18:0}O/OOC_{18:0}$, and $C_{16:0}OC_{16:0}/C_{16:0}C_{16:0}O$ positional isomer systems were used to monitor the purities of the synthesized $C_{18:0}OC_{18:0}$, $OC_{18:0}O$, and $C_{16:0}OC_{16:0}$. The construction of these calibration curves was described previously.[31] Briefly, 10 μM standards of $C_{18:0}OC_{18:0}$, $C_{18:0}C_{18:0}O$, $OC_{18:0}O$, $OOC_{18:0}$, $C_{16:0}OC_{16:0}$, and $C_{16:0}C_{16:0}O$ were used to prepare known binary mixtures of positional isomers. Standard mixtures of the following pairs of positional isomers were prepared: $C_{18:0}OC_{18:0}/C_{18:0}C_{18:0}O$, $OC_{18:0}O/OOC_{18:0}$, and $C_{16:0}OC_{16:0}/C_{16:0}C_{16:0}O$. The sum of the concentrations for the pair of positional isomers for each of the standard mixtures was 1 μM. The fractions of a positional isomer in the binary mixtures ranged from 0.00–1.00 in increments of 0.10. Each of the standard mixtures was analyzed by a targeted RP-HPLC/MS/MS method designed specifically for these three systems of positional isomers. The calibration plots were prepared by plotting the relative abundance of one of the diglyceride fragment ions as a function of fractional composition of the binary mixture. The regression statistics for these plots were used to determine the purity (in terms of positional isomers) of the synthesized $C_{18:0}OC_{18:0}$, $OC_{18:0}O$, and $C_{16:0}OC_{16:0}$.

RESULTS

Positional purity of synthesized TAGs

The detection limit for the analysis of TAGs using our RP-HPLC/ESI-MS/MS method is approximately 1–5 fmol (3:1 signal-to-noise (S/N) ratio). However, positional analysis of TAG mixtures accurate to within ±10% requires about 50–100 fmol of TAGs of a given positional isomer system.

The positional purities of the synthesized $C_{18:0}OC_{18:0}$, $OC_{18:0}O$, and $C_{16:0}OC_{16:0}$ were confirmed using the calibration curves prepared from the $C_{18:0}OC_{18:0}/C_{18:0}C_{18:0}O$, $OC_{18:0}O/OOC_{18:0}$, and $C_{16:0}OC_{16:0}/C_{16:0}C_{16:0}O$ standards purchased from Larodan. Figure 1 compares the CID spectrum of a standard solution of $OC_{18:0}O$ with that of the TAG synthesized from 1,3-diolein and stearoyl chloride. The purity of the synthesized $OC_{18:0}O$ is 98% according to a calibration plot prepared from standard mixtures of $OC_{18:0}O$ and $OOC_{18:0}$ (Larodan standards). Analysis of the synthesized $C_{18:0}OC_{18:0}$ and $C_{16:0}OC_{16:0}$ gave similar results with purities of greater than 99%. In addition, the CID spectra of several other synthesized TAGs, including $C_{12:0}OC_{12:0}$, $C_{8:0}OC_{8:0}$, $OC_{12:0}O$, and $OC_{24:0}O$, can be directly compared to the CID spectra of standard TAGs purchased from Larodan. A comparison of these data is given in Table 1. These data provide strong evidence that the synthetic strategy used in this work succeeded in producing positionally pure TAGs.

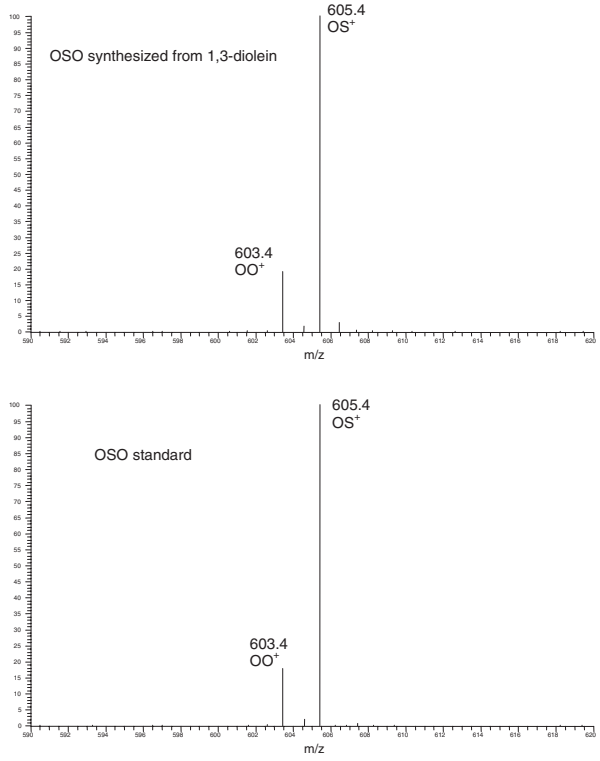

Figure 1. Comparison of the CID spectrum of the ammonium adduct of a standard OSO sample with the CID spectrum of the ammoniated TAG synthesized from 1,3-diolein and stearoyl chloride. The positional purity of the synthesized OSO is thus essentially 100%.

OXO series

Table 2 shows the relative peak intensities for the major CID products (OX^+ and OO^+) and of MH^+ in the CID spectra of the OXO-type TAGs that were synthesized in this study. The relative intensities listed in Table 2 were obtained from 25–50 spectra averaged across a chromatographic peak. Some of the TAGs were present in more than one sample, and for these TAGs the relative intensities listed are averages from multiple analyses. These data greatly add to the existing database of TAG CID spectra. More importantly, inspection of the data reveal trends as a function of fatty acid chain length, number and position of double bonds, *cis*/*trans* isomerization, and fatty acid position along the glycerol backbone, that may be useful for predicting CID spectra of TAGs.

Figure 2 shows plots of the fractional intensities of the OO^+, OX^+, and MH^+ ions as a function of chain length for the $OC_{m:0}O$ TAG series. It is evident that there are no major effects of chain length on these CID spectra. However, there is a slight, but statistically significant, decrease in the fractional intensity of OX^+ and a slight, but statistically significantly, increase in fractional intensity of MH^+ with increasing chain length. Figure 3 shows plots of the fractional intensities of the OO^+, OX^+, and MH^+ ions as a function of chain length for the $OC_{m:1}O$ TAG series. The saturated and mono-unsaturated series give essentially the same fractional intensity data for the OO^+. The distributions of the OO^+ fractional intensity data for these two groups were not significantly different according to the non-directional t-test at a CL of 90%. The average fractional intensity of the OO^+ fragment ion for these two series is 0.14 ± 0.01. However, in contrast to the saturated series, the fractional intensity of the MH^+ ion shows a slight, but statistically significant, increase with increasing chain length.

The fractional intensity of the OO^+ ion for the di-unsaturated OXO series appears to decrease significantly with increasing chain length. The data for $OC_{18:2(cc\text{-}9,12)}O$ match that of the other two series, but the fractional intensity of OO^+ for $OC_{22:2(cc\text{-}11,14)}O$ is 0.060. The fractional intensity of the MH^+ ions for the di-unsaturated subgroup is significantly greater than for the saturated and mono-unsaturated subgroups, and it also appears to increase significantly with the chain length. The fractional intensity of the MH^+ ion for $X = C_{18:2(cc\text{-}9,12)}$ and $C_{18:2(tt\text{-}9,12)}$ is 0.32 and increases to 0.37 at higher chain lengths ($C_{22:2}$).

A deeper analysis of the unsaturated OXO TAGs reveals two competing factors, namely, the total degree of unsaturation and the positions of the double bonds. In general, the fragmentation pathway yielding the MH^+ ion is favored by increasing levels of unsaturation in the TAG species. This relationship will be explored in detail below. However, the formation of OO^+ is favored when a double bond in X is placed closer to the carbonyl carbon of the fatty acid moiety. This factor can be appreciated by comparing the following OXO TAGs in Table 2: $C_{18:1(c/t\text{-}9)}$ and $C_{18:1(c/t\text{-}11)}$ with $C_{18:1(c/t\text{-}6)}$, $C_{18:3(ccc\text{-}9,12,15)}$ with $C_{18:3(ccc\text{-}6,12,15)}$, $C_{22:4(cccc\text{-}7,10,13,16)}$ with $C_{20:4(cccc\text{-}5,8,11,14)}$, and $C_{22:5(ccccc\text{-}7,10,13,16,19)}$ with $C_{20:5(ccccc\text{-}5,8,11,14,17)}$ and $C_{22:6(cccccc\text{-}4,7,10,13,16,19)}$. As an example, the $C_{18:1}$ set was explored by synthesizing TAGs using the set of $C_{18:1}$ fatty acid chlorides and the $C_{19:1}$ and $C_{20:1}$ (1,3-YYs) DAGs (in place of 1,3-diolein, OO) to synthesize $C_{19:1}C_{18:1}C_{19:1}$ and $C_{20:1}C_{18:1}C_{20:1}$ TAGs. The average fractional intensities of the YY^+ ions are 0.19 ± 02 for $C_{18:1(c/t\text{-}9)}$ and $C_{18:1(c/t\text{-}11)}$ and 0.63 ± 09 for $C_{18:1(c/t\text{-}6)}$. Similar results are revealed from the other comparisons. In addition, a quick study of Table 2 also reveals that fragmentation patterns of the TAGs are not sensitive to *cis*/*trans* configuration of the inner fatty acid moiety.

The combination of the dependence on degree of unsaturation and double-bond position can be further illustrated by looking at the subset of C_{22} fatty acid moieties in the OXO series: $C_{22:0}$, $C_{22:1(c\text{-}13)}$, $C_{22:2(cc\text{-}13,16)}$, $C_{22:3(ccc\text{-}11,14,17)}$, $C_{22:4(cccc\text{-}7,10,13,16)}$, $C_{22:5(ccccc\text{-}7,10,13,16,19)}$, and $C_{22:6(cccccc\text{-}4,7,10,13,16,19)}$. Figure 4 shows fractional intensities of the MH^+, OO^+ and XO^+ ions for the C_{22} subset as a function of degree of unsaturation. From $C_{22:0}$ to $C_{22:3(ccc\text{-}11,14,17)}$ the fractional intensities of OO^+ and XO^+ decrease as the formation of MH^+ becomes more favorable.

Table 1. Comparison of the CID data for several positionally pure TAGs synthesized in this study with CID data obtained for purchased standards

TAG	Synthesized TAGs			Larodan standards		
YXY	YY^+	XY^+	MH^+	YY^+	XY^+	MH^+
$C_{12:0}OC_{12:0}$	20	100	16	21	100	17
$C_{8:0}OC_{8:0}$	16	100	23	19	100	19
$OC_{12:0}O$	16	100	33	14	100	31
$OC_{24:0}O$	16	100	28	15	100	28

RCM

Table 2. CID data for the OXO TAGs synthesized in this study

YXY	Y	X	YY+	YX+	MH+
OXO	O	$C_{4:0}$	13.1	100.0	34.9
OXO	O	$C_{5:0}$	16.8	100.0	39.8
OXO	O	$C_{6:0}$	16.8	100.0	34.5
OXO	O	$C_{7:0}$	17.7	100.0	35.1
OXO	O	$C_{9:0}$	18.4	100.0	35.6
OXO	O	$C_{10:0}$	17.9	100.0	33.5
OXO	O	$C_{11:0}$	17.5	100.0	34.4
OXO	O	$C_{12:0}$	18.0	100.0	33.8
OXO	O	$C_{13:0}$	17.3	100.0	32.2
OXO	O	$C_{14:0}$	15.5	100.0	32.2
OXO	O	$C_{15:0}$	15.6	100.0	31.8
OXO	O	$C_{16:0}$	13.7	100.0	34.6
$C_{19:1}XC_{19:1}$	$C_{19:1(c\text{-}10)}$	$C_{16:0}$	18.0	100.0	33.7
OXO	O	$C_{17:0}$	14.9	100.0	32.0
OXO	O	$C_{18:0}$	16.9	100.0	26.4
OXO	O	$C_{19:0}$	16.1	100.0	27.5
OXO	O	$C_{20:0}$	16.9	100.0	30.0
OXO	O	$C_{21:0}$	15.6	100.0	30.2
OXO	O	$C_{22:0}$	16.4	100.0	28.6
OXO	O	$C_{23:0}$	16.8	100.0	29.7
OXO	O	$C_{24:0}$	16.6	100.0	27.6
OXO	O	$C_{11:1(c\text{-}10)}$	16.1	100.0	36.0
OXO	O	$C_{12:1(c\text{-}11)}$	14.0	100.0	35.6
OXO	O	$C_{13:1(c\text{-}12)}$	18.6	100.0	37.5
OXO	O	$C_{14:1(c\text{-}9)}$	15.8	100.0	34.0
OXO	O	$C_{14:1(t\text{-}9)}$	16.7	100.0	33.3
OXO	O	$C_{15:1(c\text{-}10)}$	16.1	100.0	36.8
OXO	O	$C_{16:1(c\text{-}9)}$	19.2	100.0	37.6
OXO	O	$C_{16:1(t\text{-}9)}$	18.2	100.0	31.5
OXO	O	$C_{17:1(c\text{-}10)}$	15.9	100.0	35.7
OXO	O	$C_{17:1(t\text{-}10)}$	17.2	100.0	35.1
$C_{19:1}XC_{19:1}$	$C_{19:1(c\text{-}10)}$	$C_{18:1(c\text{-}9)}$	17.4	100.0	32.7
$C_{20:1}XC_{20:1}$	$C_{20:1(c\text{-}11)}$	$C_{18:1(c\text{-}9)}$	21.8	100.0	35.4
$C_{19:1}XC_{19:1}$	$C_{19:1(c\text{-}10)}$	$C_{18:1(t\text{-}9)}$	17.5	100.0	38.4
$C_{20:1}XC_{20:1}$	$C_{20:1(c\text{-}11)}$	$C_{18:1(t\text{-}9)}$	22.4	100.0	36.4
$C_{19:1}XC_{19:1}$	$C_{19:1(c\text{-}10)}$	$C_{18:1(c\text{-}11)}$	18.2	100.0	36.7
$C_{20:1}XC_{20:1}$	$C_{20:1(c\text{-}11)}$	$C_{18:1(c\text{-}11)}$	21.2	100.0	42.8
$C_{19:1}XC_{19:1}$	$C_{19:1(c\text{-}10)}$	$C_{18:1(t\text{-}11)}$	16.3	100.0	38.3
$C_{20:1}XC_{20:1}$	$C_{20:1(c\text{-}11)}$	$C_{18:1(t\text{-}11)}$	21.0	100.0	41.0
$C_{19:1}XC_{19:1}$	$C_{19:1(c\text{-}11)}$	$C_{18:1(c\text{-}6)}$	72.7	100.0	30.5
$C_{20:1}XC_{20:1}$	$C_{20:1(c\text{-}10)}$	$C_{18:1(t\text{-}6)}$	55.3	100.0	26.8
$C_{19:1}XC_{19:1}$	$C_{19:1(c\text{-}11)}$	$C_{18:1(t\text{-}6)}$	60.5	100.0	28.4
OXO	O	$C_{19:1(c\text{-}10)}$	17.2	100.0	37.7
OXO	O	$C_{20:1(c\text{-}11)}$	15.4	100.0	36.9
OXO	O	$C_{22:1(c\text{-}13)}$	15.3	100.0	41.1
OXO	O	$C_{22:1(t\text{-}13)}$	15.2	100.0	35.4
OXO	O	$C_{23:1(c\text{-}14)}$	15.5	100.0	44.1
OXO	O	$C_{24:1(c\text{-}15)}$	15.4	100.0	42.7
OXO	O	$C_{18:2\ (cc\text{-}9,12)}$	15.4	100.0	54.8
OXO	O	$C_{18:2(tt\text{-}9,12)}$	14.7	100.0	54.7
OXO	O	$C_{19:2(cc\text{-}10,13)}$	13.0	100.0	60.0
OXO	O	$C_{20:2(cc\text{-}11,14)}$	11.4	100.0	61.1
OXO	O	$C_{22:2(cc\text{-}13,16)}$	10.6	100.0	65.4
OXO	O	$C_{18:3(ccc\text{-}6,9,12)}$	45.7	62.2	100.0
OXO	O	$C_{18:3(ccc\text{-}9,12,15)}$	15.9	67.0	100.0
OXO	O	$C_{20:3(ccc\text{-}11,14,17)}$	9.6	59.1	100.0
OXO	O	$C_{20:3(ccc\text{-}8,11,14)}$	12.3	58.4	100.0
OXO	O	$C_{22:3(ccc\text{-}13,16,19)}$	8.8	59.7	100.0
OXO	O	$C_{20:4(cccc\text{-}5,8,11,14)}$	76.4	100.0	100.0
OXO	O	$C_{22:4(cccc\text{-}7,10,13,16)}$	12.6	38.8	100.0
OXO	O	$C_{20:5(ccccc\text{-}5,8,11,14,17)}$	100.0	54.2	79.5
OXO	O	$C_{22:5(ccccc\text{-}7,10,13,16,19)}$	35.5	55.8	100.0
OXO	O	$C_{22:6(cccccc\text{-}4,7,10,13,16,19)}$	100.0	38.2	53.3

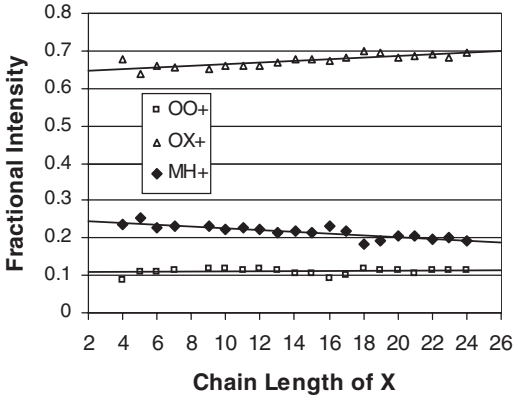

Figure 2. Fractional ion intensities of the OO^+, OX^+, and MH^+ fragment ions as a function of fatty acid chain length for the OXO saturated data set. Fractional intensities of OO^+, OX^+, and MH^+ are given by $I_{OO+}/(I_{OO+} + I_{OX+} + I_{MH+})$, $I_{OX+}/(I_{OO+} + I_{OX+} + I_{MH+})$, and $I_{MH+}/(I_{OO+} + I_{OX+} + I_{MH+})$, respectively.

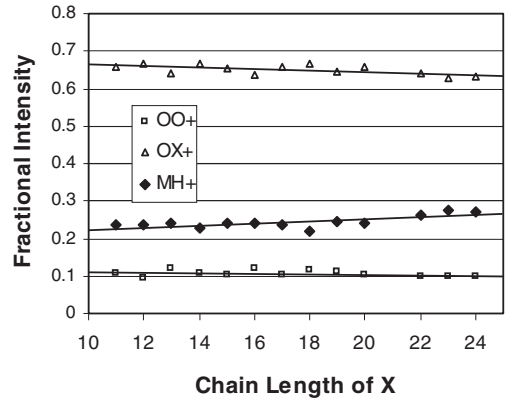

Figure 3. Fractional ion intensities of the OO^+, OX^+, and MH^+ ions as a function of fatty acid chain length for the OXO mono-unsaturated data set. Fractional intensities of OO^+, OX^+, and MH^+ are given by $I_{OO+}/(I_{OO+} + I_{OX+} + I_{MH+})$, $I_{OX+}/(I_{OO+} + I_{OX+} + I_{MH+})$, and $I_{MH+}/(I_{OO+} + I_{OX+} + I_{MH+})$, respectively.

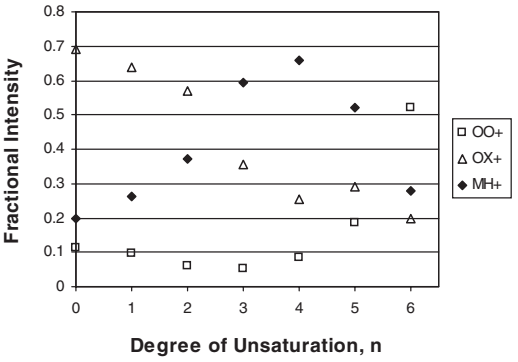

Figure 4. Fractional ion intensities of the OO^+, OX^+, and MH^+ ions as a function of fatty acid degree of unsaturation for the $C_{22:n}$ TAGs. Fractional intensities of OO^+, OX^+, and MH^+ are given by $I_{OO+}/(I_{OO+} + I_{OX+} + I_{MH+})$, $I_{OX+}/(I_{OO+} + I_{OX+} + I_{MH+})$, and $I_{MH+}/(I_{OO+} + I_{OX+} + I_{MH+})$, respectively.

However, the fractional intensity of OO^+ increases dramatically with the presence of additional double bonds closer to the carbonyl carbon in $C_{22:4(cccc\text{-}7,10,13,16)}$, $C_{22:5(ccccc\text{-}7,10,13,16,19)}$, and $C_{22:6(cccccc\text{-}4,7,10,13,16,19)}$.

YOY series

Table 3 shows the relative peak intensities for the major CID products, YO^+, YY^+, and MH^+, in the CID spectra of the YOY-type TAGs that were synthesized in this study. Figure 5 shows plots of the fractional intensities of the YY^+, OY^+, and MH^+ fragment ions as a function of chain length for the $C_{m:0}OC_{m:0}$ subset. The fractional intensities of the YY^+ ions increase as a function of chain length for this subset; 0.14 at low chain length ($C_{8:0}$) up to 0.17 at longer chain lengths ($C_{22:0}$). The fractional intensity of the MH^+ ion decreases significantly with the chain length of $C_{m:0}$ for the saturated subset, i.e., 0.14 at low chain length ($C_{8:0}$) steadily declining to 0.06 at higher chain lengths ($C_{22:0}$). The fractional intensities of the YO^+ ions increase as a function of chain length for this subset: 0.73 at low chain length ($C_{8:0}$) up to 0.77 at longer chain lengths ($C_{22:0}$).

Figure 6 shows plots of the fractional intensities of the YY^+, OY^+, and MH^+ ions as a function of chain length for the $C_{m:1}OC_{m:1}$ subset. The fractional intensities of the YY^+ ions increase as a function of chain length for this subset, i.e., 0.11 at low chain length ($C_{11:1}$) up to 0.15 at longer chain lengths ($C_{22:1}$). The fractional intensity of the MH^+ ion increases significantly with the chain length of $C_{m:1}$ for the mono-unsaturated subset: 0.20 at low chain length ($C_{11:1}$) and steadily rising to 0.25 at higher chain lengths ($C_{22:1}$). The fractional intensities of the YO^+ ions steadily decrease with chain length for this subset: 0.72 at low chain length ($C_{11:1}$) down to 0.60 at longer chain lengths ($C_{22:1}$).

Several striking comparisons can be made between the saturated and mono-unsaturated YOY subsets. The slopes and intercepts for each of the fragment ions (YY^+, YO^+, and MH^+) from Figs. 5 and 6 can be directly compared. The slope for the YY^+ regression of the mono-unsaturated subset is significantly larger than the corresponding slope for the saturated subset, but the fractional intensities of the YY^+ ions are greater for the saturated series at comparable chain lengths of Y. The fractional intensities of the MH^+ ions are considerably greater for the mono-unsaturated subset than for the saturated subset. In addition, the saturated and mono-unsaturated YOY subsets show opposite trends in the fractional intensity of MH^+ with chain length; the slope of the MH^+ regression line for the saturated subset is strongly negative while that for the mono-unsaturated subset is significantly positive. A similar comparison of the YO^+ trend lines reveals that the fractional intensities at lower chain length are about 0.70 for both subsets. However, the slope of the YO^+ regression line for the saturated subset is significantly positive and that for the mono-unsaturated subset is strongly negative.

Analysis of the YOY TAGs containing unsaturated fatty acids in the Y position reveals a dependence on degree of unsaturation and double-bond position on the fragmentation pattern similar to that described for the OXO series. The formation of the MH^+ ion becomes more favorable relative to YY^+ and YO^+ as the degree of unsaturation in the TAG is

RCM

Table 3. CID data for the YOY TAGs synthesized in this study

YXY	Y	X	YY^+	YX^+	MH^+
YOY	$C_{8:0}$	O	17.7	100.0	19.7
YOY	$C_{9:0}$	O	23.2	100.0	16.4
YOY	$C_{10:0}$	O	16.5	100.0	17.7
YOY	$C_{11:0}$	O	19.9	100.0	17.0
YOY	$C_{12:0}$	O	20.1	100.0	14.6
YOY	$C_{13:0}$	O	15.6	100.0	12.7
YOY	$C_{14:0}$	O	19.9	100.0	14.0
YOY	$C_{15:0}$	O	20.1	100.0	13.6
YOY	$C_{16:0}$	O	23.5	100.0	12.8
$YC_{19:1}Y$	$C_{16:0}$	$C_{19:1(c\text{-}10)}$	20.7	100.0	15.3
YOY	$C_{17:0}$	O	20.9	100.0	14.2
YOY	$C_{18:0}$	O	22.2	100.0	11.2
YOY	$C_{19:0}$	O	20.3	100.0	10.0
YOY	$C_{20:0}$	O	21.9	100.0	8.6
YOY	$C_{21:0}$	O	20.9	100.0	10.1
YOY	$C_{22:0}$	O	22.7	100.0	7.3
YOY	$C_{11:1(c\text{-}10)}$	O	15.9	100.0	30.7
YOY	$C_{12:1(c\text{-}11)}$	O	19.8	100.0	32.8
YOY	$C_{14:1(c\text{-}9)}$	O	16.7	100.0	29.2
YOY	$C_{16:1(c\text{-}9)}$	O	17.6	100.0	30.3
YOY	$C_{16:1(t\text{-}9)}$	O	15.5	100.0	34.0
YOY	$C_{17:1(c\text{-}10)}$	O	20.1	100.0	36.4
$Y_{C19:1}Y$	$C_{18:1(c\text{-}9)}$	$C_{19:1(c\text{-}10)}$	17.4	100.0	37.0
$YC_{20:1}Y$	$C_{18:1(t\text{-}9)}$	$C_{20:1(c\text{-}11)}$	27.4	100.0	39.8
$Y_{C19:1}Y$	$C_{18:1(c\text{-}11)}$	$C_{19:1(c\text{-}10)}$	26.3	100.0	42.1
$YC_{20:1}Y$	$C_{18:1(c\text{-}11)}$	$C_{20:1(c\text{-}11)}$	20.4	100.0	42.5
$Y_{C19:1}Y$	$C_{18:1(c\text{-}6)}$	$C_{19:1(c\text{-}10)}$	7.2	100.0	8.8
$YC_{20:1}Y$	$C_{18:1(c\text{-}6)}$	$C_{20:1(c\text{-}11)}$	5.3	100.0	8.3
$Y_{C19:1}Y$	$C_{18:1(t\text{-}6)}$	$C_{19:1(c\text{-}10)}$	11.8	100.0	12.3
$YC_{20:1}Y$	$C_{18:1(t\text{-}6)}$	$C_{20:1(c\text{-}11)}$	8.3	100.0	11.3
YOY	$C_{20:1(c\text{-}11)}$	O	23.3	100.0	39.0
YOY	$C_{22:1(c\text{-}13)}$	O	28.0	100.0	43.0
YOY	$C_{22:1(t\text{-}13)}$	O	23.5	100.0	45.5
YOY	$C_{24:1(c\text{-}15)}$	O	24.6	100.0	41.5
YOY	$C_{18:2(cc\text{-}9,12)}$	O	17.1	33.2	100.0
YOY	$C_{18:2(tt\text{-}9,12)}$	O	17.9	32.9	100.0
YOY	$C_{19:2(cc\text{-}10,13)}$	O	13.8	29.7	100.0
YOY	$C_{20:2(cc\text{-}13,16)}$	O	15.2	30.9	100.0
YOY	$C_{18:3(ccc\text{-}9,12,15)}$	O	20.0	28.0	100.0
YOY	$C_{18:3(ccc\text{-}6,9,12)}$	O	16.3	60.8	100.0
YOY	$C_{20:3(ccc\text{-}8,11,14)}$	O	15.3	21.5	100.0
YOY	$C_{20:3(ccc\text{-}11,14,17)}$	O	16.2	18.4	100.0
YOY	$C_{20:4(cccc\text{-}5,8,11,4)}$	O	7.6	100.0	52.2

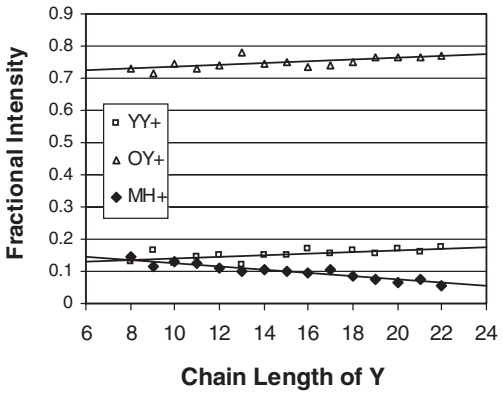

Figure 5. Fractional ion intensities of the YY^+, OY^+, and MH^+ ions as a function of fatty acid chain length for the YOY saturated data set. Fractional intensities of YY^+, OY^+, and MH^+ are given by $I_{YY+}/(I_{YY+} + I_{OY+} + I_{MH+})$, $I_{OY+}/(I_{YY+} + I_{OY+} + I_{MH+})$, and $I_{MH+}/(I_{YY+} + I_{OY+} + I_{MH+})$, respectively.

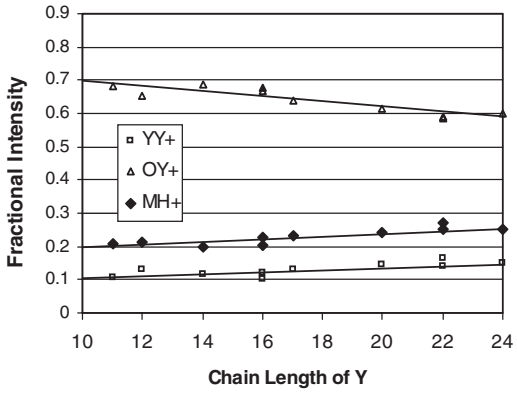

Figure 6. Fractional ion intensities of the YY^+, OY^+, and MH^+ ions as a function of fatty acid chain length for the YOY monounsaturated data set. Fractional intensities of YY^+, OY^+, and MH^+ are given by $I_{YY+}/(I_{YY+} + I_{OY+} + I_{MH+})$, $I_{OY+}/(I_{YY+} + I_{OY+} + I_{MH+})$, and $I_{MH+}/(I_{YY+} + I_{OY+} + I_{MH+})$, respectively.

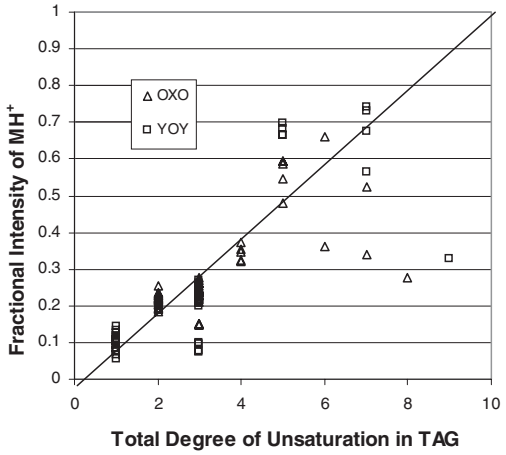

Figure 7. Fractional ion intensities of the MH^+ fragment ion as a function of degree of unsaturation for the OXO and YOY data sets. Fractional intensities of MH^+ are given by $I_{MH+}/(I_{YY+} + I_{OY+} + I_{MH+})$.

increased. For example, the fractional intensities of MH^+ for the di-unsaturated subgroup are much greater, at 0.67 ± 0.02. However, the formation of YO^+ is enhanced greatly when a double bond in Y is placed closer to the carbonyl carbon of the fatty acid moiety. This factor can be appreciated by comparing the following YOY TAGs in Table 3: $C_{18:1(c/t\text{-}9)}$ and $C_{18:1(c/t\text{-}11)}$ with $C_{18:1(c/t\text{-}6)}$, $C_{18:3(ccc\text{-}9,12,15)}$ with $C_{18:3(ccc\text{-}6,12,15)}$, and $C_{20:3(cccc\text{-}8,11,14)}$ with $C_{20:4(cccc\text{-}5,8,11,14)}$. As an example, the fractional intensities of the YO^+ ions for $C_{18:3(ccc\text{-}9,12,15)}$ and $C_{18:3(ccc\text{-}6,12,15)}$ YOY TAGs are 0.19 and 0.34, respectively.

Comparison of *cis*/*trans* Y pairs in the YOY series is not straightforward and the effect of *cis*/*trans* configuration of the outer fatty acid moieties remains inconclusive.

Degree of unsaturation

As noted above, higher levels of unsaturation in TAGs favor the formation of MH^+. This trend has also been noted in APCI experiments. An illustration of this effect is given in Fig. 7, where the fractional intensity of the MH^+ ion is plotted vs. the total degree of unsaturation for all of the TAGs listed in Tables 2 and 3. There is a strong correlation between the fractional intensity of MH^+ and the degree of unsaturation. The major outlier points are TAGs that contain unsaturated fatty acids with double bonds positioned close to the carbonyl carbon. With the exclusion of these data points, linear regression analysis gives a multiple correlation coefficient of 0.91. Thus, the fractional intensity of MH^+ is dependent on the total level of unsaturation in a predictable fashion.

Predicting fragmentation patterns

Factors that determine the fragmentation patterns of TAGs have been examined in this work. The trends revealed from analysis of these data may be useful in predicting fragmentation patterns for other TAGs. We used several of the purchased TAG standards, and several YOX-type TAGs synthesized from 2-oleoylglycerol, to investigate the possibility of using the trends in the figures presented above to predict the fragmentation patterns. The trendlines shown in Figs. 2, 3, 5 and 6 were used to predict the relative intensities of fragment ions in the CID spectra of $C_{24:0}OC_{24:0}$, $OC_{8:0}O$, $C_{16:0}OC_{18:0}$, $C_{16:0}OC_{20:0}$, $C_{12:0}OC_{22:0}$, $C_{12:0}OC_{24:0}$, $C_{22:0}OC_{24:0}$, and $C_{18:2(cc\text{-}9,12)}OC_{18:0}$. The regression statistics from these trendlines are given in Table 4. The CID spectrum of $C_{24:0}OC_{24:0}$ was predicted using the trendlines for the saturated YOY subset, and the CID spectrum of $OC_{8:0}O$ was predicted using the trendlines for the saturated OXO subset. Predicting the CID spectra for YOX-type TAGs is more complex. The general scheme for predicting the fragmentation patterns of the YOX-type TAGs is outlined below:

Step 1: Calculate $I_{(XX+)XOX}$, $I_{(YY+)YOY}$, $I_{(MH+)XOX}$, $I_{(MH+)YOY}$, $I_{(OX+)XOX}$, and $I_{(OY+)YOY}$ using the regression parameters from Fig. 5.

$$I_{YX+} = \{I_{(XX+)XOX} + I_{(YY+)YOY}\}/2$$

$$I_{MH+} = \{I_{(MH+)XOX} + I_{(MH+)YOY}\}/2$$

Step 2: $I_{(OY+)YOY}$ and $I_{(OX+)XOX}$ are measures of the propensity to lose Y and X, respectively. Thus, $I_{(OY+)YOY}/I_{(OX+)XOX}$ is a measure of the I_{OX+}/I_{OY+} ratio in the CID spectrum of YOX.

$$I_{OX+} = \{I_{(OY+)YOY}/I_{(OX+)XOX}\} * I_{OY+}$$

$$I_{OX+} + I_{OY+} = 1 - I_{YX+} - I_{MH+}$$

$$\{I_{(OY+)YOY}/I_{(OX+)XOX}\} * I_{OY+} + I_{OY+} = 1 - I_{YX+} - I_{MH+}$$

$$I_{OY+} = \{1 - I_{YX+} - I_{MH+}\}/\{1 + I_{(OY+)YOY}/I_{(OX+)XOX}\}$$

$$I_{OX+} = 1 - I_{YX+} - I_{MH+} - I_{OY+}$$

Table 4. Regression parameters from the plots in Figs. 2, 3, 5 and 6, used in predicting fragmentation patterns

Series	Subseries	Fragment	Slope	Intercept	Standard error of regression
OXO	Saturated	OX^+	0.0021 ± 0.0004	0.64 ± 0.01	0.010
OXO	Saturated	OO^+	0.0002 ± 0.0003	0.107 ± 0.005	0.009
OXO	Saturated	MH^+	-0.0024 ± 0.0004	0.250 ± 0.006	0.010
OXO	Monousat.	OX^+	-0.0020 ± 0.0008	0.685 ± 0.014	0.011
OXO	Monounsat	OO^+	-0.0007 ± 0.0006	0.116 ± 0.012	0.009
OXO	Monounsat	MH^+	0.0028 ± 0.0008	0.197 ± 0.015	0.012
YOY	Saturated	OY^+	0.0027 ± 0.0008	0.708 ± 0.013	0.014
YOY	Saturated	YY^+	0.0025 ± 0.0008	0.115 ± 0.013	0.013
YOY	Saturated	MH^+	-0.0052 ± 0.0005	0.177 ± 0.008	0.008
YOY	Monounsat	OY^+	-0.0077 ± 0.0014	0.786 ± 0.025	0.019
YOY	Monounsat	YY^+	0.0033 ± 0.0009	0.072 ± 0.017	0.013
YOY	Monounsat	MH^+	0.0044 ± 0.0009	0.153 ± 0.016	0.012

RCM

For example, the CID spectrum of $C_{16:0}OC_{20:0}$ was predicted using the fractional intensity data for $C_{16:0}OC_{16:0}$ and $C_{20:0}OC_{20:0}$ obtained from regression parameters in Table 3. The intensities of $C_{16:0}C^{+}_{20:0}$ and MH^+ were calculated from the average fractional intensities of YY^+ and MH^+, respectively, for $C_{16:0}OC_{16:0}$ and $C_{20:0}OC_{20:0}$.

Step 1:

$$I_{C16:0C20:0+} = \{I_{(16:0C16:0+)C16:0OC16:0} + I_{(20:0C20:0+)C20:0OC20:0}\}/2 = (0.155 + 0.165)/2 = 0.160$$

$$I_{MH+} = \{I_{(MH+)C16:0OC16:0} + I_{(MH+)C20:0OC20:0}\}/2 = (0.094 + 0.074)/2 = 0.084$$

Step 2:

$$I_{OC16:0+} + I_{OC20:0+} = 1 - I_{C16:0C20:0+} - I_{MH+} = 0.76$$

$$I_{O20:0+} = \{I_{(O160+)C16:0OC16:0} + I_{(OC20:0+)C20:0OC20:0}\} * I_{OC16:0+} = (0.7511/0.762)I_{OC16:0+} = 0.986\ I_{OC16:0+}$$

$$I_{O16:0+} + 0.986 * I_{OC16:0+} = 1 - I_{C16:0C20:0+} - I_{MH+}$$

$$I_{O16:0+} = \{1 - 0.160 - 0.084\}/\{1 + 0.986\} = 0.381$$

$$I_{O20:0+} = 1 - 0.160 - 0.084 - 0.381 = 0.375$$

Step 3: Normalize by setting the most abundant fragment to an intensity of 100

$$I_{C16:0C20:0+} = 100 * (0.160/0.381) = 42$$

$$I_{MH+} = 100 * (0.084/0.381) = 22$$

$$I_{O16:0+} = 100 * (0.381/0.381) = 100$$

$$I_{O20:0+} = 100 * (0.375/0.381) = 98$$

Table 5 compares the CID spectra predicted from these calculations with the CID spectra obtained from the Larodan standards and XOY-type TAGs. In each case the predicted spectrum matches the acquired data fairly well. The analysis of $C_{18:2(cc\text{-}9,12)}OC_{18:0}$ is complicated by the different levels of unsaturation in the reference TAGs, $C_{18:2(cc\text{-}9,12)}OC_{18:2(cc\text{-}9,12)}$ and $C_{18:0}OC_{18:0}$. In this case, Fig. 7 was used to estimate the fractional intensity of the MH^+ fragment from $C_{18:2(cc\text{-}9,12)}OC_{18:0}$. Nevertheless, the predicted intensities are in fair agreement with the experimental data.

DISCUSSION

The trends revealed in the data can largely be explained based on gas-phase basicities and ammonium affinities. Gas-phase basicities of olefins and esters are similar, and therefore it is reasonable to expect that ammoniation can take place at the carbonyl groups on each fatty acid moiety as well as at any double bond positioned along a given fatty acid chain. It has been reported and verified in some of our experiments that MS/MS of TAGs containing three saturated fatty acid moieties produces negligible amounts of MH^+ ions. Therefore, it is likely that ammoniation at the carbonyl groups produces DAG^+ ions exclusively upon CID. Any reasonable mechanism for the formation of the DAG^+ fragment ions upon CID would require that the ammonium ion be adjacent to the carbonyl. Therefore, we hypothesize that, when ammoniation takes place at a double bond along one of the fatty acid chains, fragmentation likely results exclusively in MH^+ ions. Figure 7 supports this argument since an increase in the total number of double bonds enhances the relative formation of MH^+ and the y-intercept is close to zero (-0.02 ± 0.03 @ 95% CL). Figure 8 summarizes this hypothesis by illustrating a possible reaction scheme for the formation and dissociation of the ammoniated TAG species. The $C_{18:2(cc\text{-}9,12)}OC_{18:0}$ TAG species is used as a convenient example in this illustration. Ammoniation at carbonyl groups produces the OS^+, LS^+, and OL^+ ions, while ammoniation at the double bonds of L and O produces MH^+ upon CID.

It has been observed previously that loss of the fatty acid from the center position is unfavorable in the CID of TAGs. This is also observed in the CID spectra of the TAGs analyzed in this work. The plots for the saturated and monounsaturated YOY series show a much greater sensitivity to chain length than the plots for the OYO series. It is likely that ammoniation at the center position is hindered thus prohibiting the formation of YY^+/OO^+, which would explain the limited dependence on chain length for the OXO series. However, the fractional intensities of MH^+ ions do show a dependence on degree of unsaturation, which suggests that ammoniation at a double bond is not as hindered by its location on the center fatty acid.

The trends for the MH^+ ions in Figs. 2 and 4 can be explained based on the ability of the longer chain lengths to enhance solvation of the ammonium ion at the carbonyl

Table 5. Comparison of the predicted intensities of the CID fragment ions with the CID data acquired from purchased standards and TAGs synthesized from 2-oleoylglycerol

	Predictions				Standards			
OXO		OO^+	OX^+	MH^+		OO^+	OX^+	MH^+
$OC_{8:0}O$[a]		17	100	35		17	100	34
YOY		YY^+	OY^+	MH^+		YY^+	OY^+	MH^+
$C_{24:0}OC_{24:0}$[a]		23	100	7		18	100	10
YOX	OY^+	YX^+	OX^+	MH^+	OY^+	YX^+	OX^+	MH^+
$C_{12:0}OC_{22:0}$[b]	100	41	98	23	90	45	100	23
$C_{12:0}OC_{24:0}$[b]	100	42	97	22	89	43	100	21
$C_{16:0}OC_{18:0}$[a]	100	42	99	24	99	41	100	23
$C_{16:0}OC_{20:0}$[a]	100	42	99	22	100	42	99	23
$C_{22:0}OC_{24:0}$[b]	100	45	99	15	100	46	98	17
$C_{18:2(c\text{-}9)}OC_{18:0}$[b]	100	41	80	70	100	26	68	65

[a] Standards purchased from Larodan.
[b] TAGs synthesized from 2-oleoylglycerol.

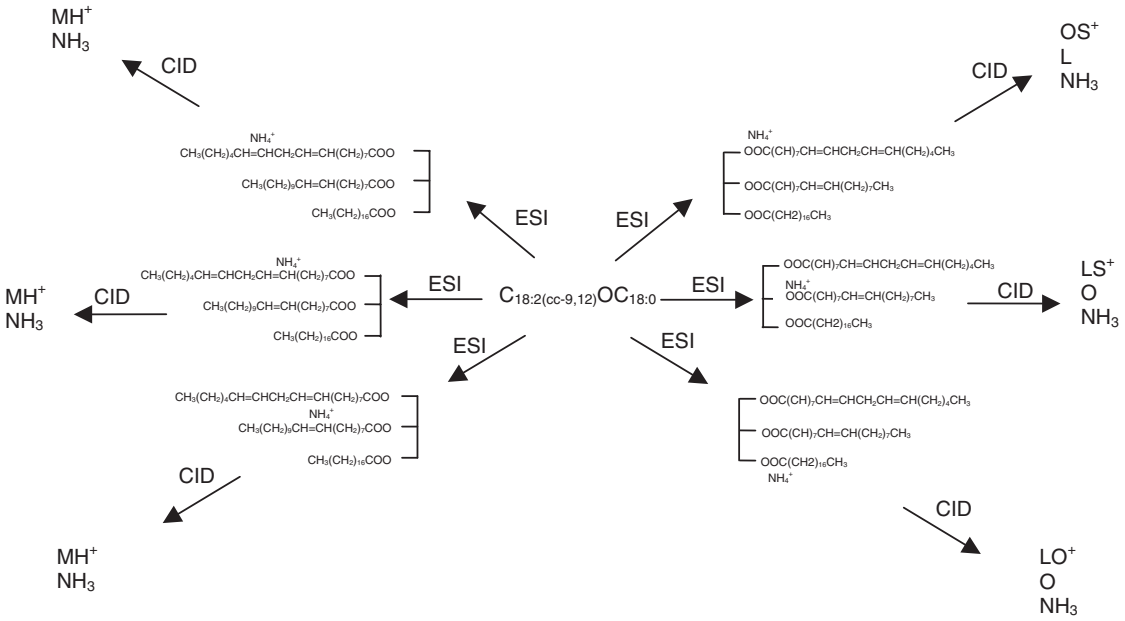

Figure 8. Proposed reaction scheme for the electrospray ionization and subsequent collision-induced decomposition of LOS. When ammoniation takes place at the carbonyl carbon, CID favors loss of the fatty acid moiety producing the corresponding DAG^+ fragment. When ammoniation takes place at a double bond, CID produces MH^+. Abbreviations: L, $C_{18:2(cc\text{-}9,12)}$; O, $C_{18:1(c\text{-}9)}$; S, $C_{18:0}$.

groups, producing a relative decrease in the abundance of MH^+. The opposite trends observed for the mono-unsaturated series, shown in Figs. 3 and 5, suggest the longer chain lengths have an even greater stabilization effect on ammonium groups at the double bonds.

As illustrated by the present data, the relative intensities of the fragment ions are sensitive to the presence of double bonds positioned near the carbonyl group along the fatty acid chain. Some added stability that these adjacent double bonds may give to the solvation of the ammonium ion at the carbonyl group of the fatty acid moiety might account for this phenomenon. By application of our working model outlined in Fig. 8, ammoniation at the carbonyl group of X in OXO produces OO^+, and ammoniation at the carbonyl groups of Y's in YOY produces YO^+. Therefore, one would expect that added stability from an adjacent double bond in X or Y would enhance the relative formation of OO^+ in the OXO TAGs and OY^+ in the YOY TAGs, which is in agreement with our data.

The future vision for this project is the development of an automated method for the comprehensive analysis of complex TAG mixtures. The creation of such a platform depends on the design of smart software that would integrate TAG quantification of individual positional isomers with retention time prediction, chromatographic peak deconvolution, and library matching. Chromatographic peak deconvolution will be necessary for the analysis of complex mixtures that often contain some co-eluting compounds. Aspects of such software may be similar to those of the MSPECTRA software developed by Kurvinen *et al*.[49] However, critical to the development of a rugged method will be the development of a library of derived CID spectra. This library will be constructed from models that predict fragmentation patterns. The present successful application of the regression parameters from the OXO and YOY data series in predicting the CID spectra of a limited set of positionally pure TAGs of composition OXO, YOY, and YOX suggests that the development of a robust library consisting of derived spectra is an achievable goal.

The software visualized above could be designed for integration into the commercial software of the LCQ ion trap used in the present work, or as a stand-alone software package. A stand-alone software package possibly could also be designed to work with a triple-quadrupole platform and/or in conjunction with an APCI-MS method. There may be significant differences in the CID data acquired using an ion trap vs. the CID data acquired using a triple quadrupole. An analysis similar in scope to the work described in this paper would then be performed using a triple-quadrupole instrument to extend the utility of the proposed software package. In addition, the development of a comprehensive APCI-MS database modeled after the approach described here could open the door for similar APCI-MS software. Perhaps a single software package could be designed to permit the selection of the applicable instrument and method (ion trap/quadrupole, ESI-MS/MS/APCI-MS) used in the analysis.

Future work will concentrate on investigating similar systems where common fatty acids moieties, such as palmitate, stearate, linoleate, and arachodonate, will be used in place of oleate. The collection of these data will provide a sound basis for the development of a model that can predict the fragmentation patterns of all species of TAGs. Also, racemic mixtures of the positional isomers of the TAGs studied in this work, as well as other YXY-type TAGs studied in the future, will be prepared. The linear relationship

between the fractional intensities of the DAG fragment ions and the binary compositions of positional isomers can be exploited by using the data from the YXY-type TAGs in conjunction with the data from racemic mixtures (33% YXY/66% YYX) to predict the fractional intensities in the CID spectra of YYX. As a result, the key reference data for all of these positional isomer systems could be incorporated into the models used to predict fragmentation patterns.

Acknowledgement

Acknowledgment is made to the donors of The American Chemical Society Petroleum Research Fund for support of this research.

REFERENCES

1. Hunter JE. *Lipids* 2001; **36**: 655.
2. Filer LJ Jr, Mattson FH, Fomon SJ. *J. Nutr.* 1969; **99**: 293.
3. Small DM. *Annu. Rev. Nutr.* 1991; **11**: 413.
4. Lien EL, Boyle FG, Yuhas R, Tomarelli RM, Quinlan P. *J. Pediatr. Gastroenterol. Nutr.* 1997; **25**: 167.
5. Aoyama T, Fukui K, Taniguchi K, Nagaoka S, Yamaoto T, Hashimoto Y. *J. Nutr.* 1996; **126**: 225.
6. Kritchevsky D. *Nutr. Rev.* 1988; **46**: 177.
7. Redgrave TG, Kodali DR, Small DM. *J. Biol. Chem.* 1988; **263**: 5118.
8. Pufal DA, Quinlan PT, Salter AM. *Biochim. Biophys. Acta* 1995; **1258**: 41.
9. Renaud SC, Ruf JC, Petithory D. *J. Nutr.* 1995; **125**: 229.
10. Cherian G, Sim JS. *Nutrition* 1996; **12**: 8.
11. Decker EA. *Nutr. Rev.* 1996; **54**: 108.
12. Aoe S, Yamamura J, Matsuyama H, Hase M, Shiota M, Miura S. *J. Nutr.* 1997; **127**: 1269.
13. Summers LK, Fielding BA, Ilic V, Quinlan PT, Frayn KN. *Br. J. Nutr.* 1998; **79**: 141.
14. Kritchevsky D, Tepper SA. *Exp. Mol. Pathol.* 1967; **6**: 394.
15. Kritchevsky D, Tepper SA, Vesselinovitch D, Wissler RW. *Atherosclerosis* 1973; **17**: 225.
16. Kritchevsky D, Tepper SA, Kuksis A, Eghtedary K, Klurfeld DM. *J. Nutr. Biochem.* 1998; **9**: 582.
17. Kritchevsky D, Tepper SA, Wright S, Kuksis A, Hughes TA. *Nutr. Res.* 1998; **18**: 259.
18. Kritchevsky D, Tepper SA, Chen SC, Meijer GW, Krauss RM. *Lipids* 2000; **35**: 621.
19. Kritchevsky D, Tepper SA, Kuksis A, Wright S, Czarnecki SK. *Nutr. Res.* 2000; **20**: 887.
20. Kubow S. *J. Nutr. Biochem.* 1996; **7**: 530.
21. Ikeda I, Yoshida H, Tomooka M, *et al. Lipids* 1998; **33**: 897.
22. Byrdwell WC, Emken EA, Neff WE, Adlof RO. *Lipids* 1996; **31**: 919.
23. Byrdwell WC, Emken EA. *Lipids* 1995; **30**: 173.
24. Byrdwell WC, Neff WE, List GR. *J. Agric. Food Chem.* 2001; **49**: 446.
25. Mottram HR, Woodbury SE, Evershed RP. *Rapid Commun. Mass Spectrom.* 1997; **11**: 1240.
26. Mottram HR, Crossman ZM, Evershed RP. *Analyst* 2001; **126**: 1018.
27. Mottram HR, Evershed RP. *J. Chromatogr. A* 2001; **926**: 239.
28. Holcapek M, Jandera P, Zderadicka P, Hruba L. *J. Chromatogr. A* 2003; **1010**: 195.
29. Fauconnot L, Hau J, Aeschlimann JM, Fay LB, Dionisi F. *Rapid Commun. Mass Spectrom.* 2004; **18**: 218.
30. Hvattum E. *Rapid Commun. Mass Spectrom.* 2001; **15**: 187.
31. Malone M, Evans JJ. *Lipids* 2004; **39**: 273.
32. Byrdwell WC, Neff WE. *Rapid Commun. Mass Spectrom.* 2002; **16**: 300.
33. Kallio H, Laakso P, Huopalahti R, Linko RR, Oksman P. *Anal. Chem.* 1989; **61**: 698.
34. Brockerhoff H. *J. Lipid Res.* 1965; **79**: 10.
35. Brockerhoff H, Yurkowski M. *J. Lipid Res.* 1966; **7**: 62.
36. Brockerhoff H, Hoyle RJ, Wolmark N. *Biochim. Biophys. Acta* 1966; **116**: 67.
37. Brockerhoff H. *J. Lipid Res.* 1967; **8**: 167.
38. Myher JJ, Kuksis A, Breckenridge WC, Little JA. *Lipids* 1984; **19**: 683.
39. Slakey PM, Lands WEM. *Lipids* 1967; **3**: 30.
40. Akesson B. *Eur. J. Biochem.* 1969; **9**: 463.
41. Christie WW, Moore JH. *Biochim. Biophys. Acta* 1969; **176**: 445.
42. Christie WW, Moore JH. *Biochim. Biophys. Acta* 1970; **218**: 83.
43. Christie WW, Moore JH. *Biochim. Biophys. Acta* 1970; **210**: 46.
44. Christie WW, Clegg RA, Calvert DT, Noble RC. *Lipids* 1984; **19**: 982.
45. Miyazawa T, Ito S, Fujino Y. *J. Nutr. Sci. Vitaminol. (Tokyo)* 1975; **21**: 137.
46. Myher JJ, Kuksis A, Geher K, Park PW, Diersen-Schade DA. *Lipids* 1996; **31**: 207.
47. Kallio H, Yli-Jokipii K, Kurvinen JP, Sjovall O, Tahvonen R. *J. Agric. Food Chem.* 2001; **49**: 3363.
48. Kurvinen JP, Mu H, Kallio H, Xu X, Hoy CE. *Lipids* 2001; **36**: 1377.
49. Kurvinen JP, Rua P, Sjovall O, Kallio H. *Rapid Commun. Mass Spectrom.* 2001; **15**: 1084.